impacting the 10-yr design objective in the storage phase: the propellant status detector dropout distance (Fig. 5). The concern lies in the fact that the population of values appears to be concentrated at the upper ageout alert limit.

The trend of PSD dropout distance as a function of age is not significant, and the low determination coefficient suggests little or no time dependency. Moreover, no significant aging mechanisms have been identified to postulate an aging trend. Assuming, however, that an aging trend does materialize, and does result in intersection of the 3-sigma prediction limit and upper ageout alert limit within 10 yr, the predicted impact on the mission could be failure to signal low propellant volume. The actual probability of starting a mission with less than the required propellant volume is presently 10^{-15}, based on actual leakage rate measurements. Moreover, the probability of corrosion creating a sudden gross leakage problem is equally unlikely, given the absence of a significant decreasing trend in corrosion inhibitor (nitric oxide) and the absence of visible evidence of corrosion to date. In view of these facts, the data in Fig. 5 is considered of little significance at the present time.

Flight Phase

Two distinct failure types are postulated in the flight phase: the sudden catastrophic failure, the probability of which is greatest during the boost, stage separation, and immediate post-boost phases of the mission; and the flight performance failure, which is characterized by an inability to perform the required flight maneuvers with sufficient accuracy.

Evidence to date shows that only the RF current attenuation for the pyrotechnic control cable at 10 MHz frequency (Fig. 6), could possibly be interpreted as a parameter of concern and for the same reason previously cited: the population of values is concentrated at the ageout alert limit. The significant trend and fairly high determination coefficient may be ignored in this case, because it is suspected that the post storage data, having been measured on cables which were stressed, show lower attenuation values than the zero time data, which reflect the unstressed cables. Moreover, no aging mechanisms have been identified to account for the significant decrease in attenuation. This, of course, does not alter the concern that a true aging trend would produce

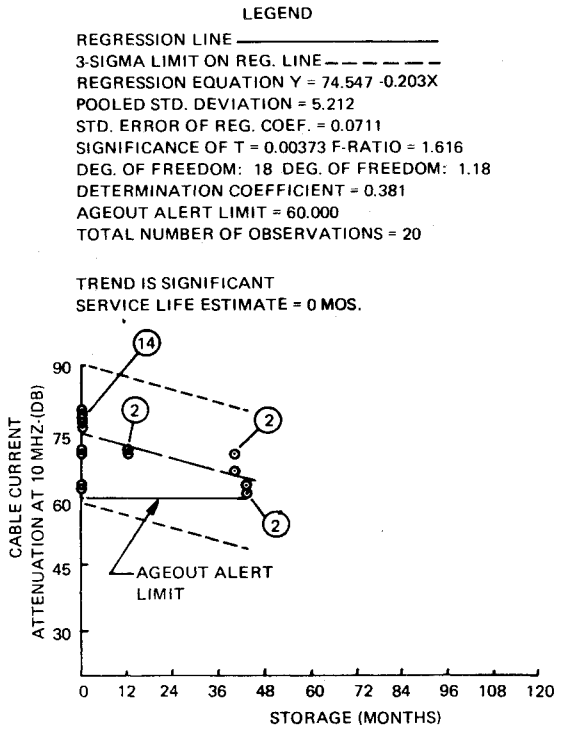

Fig. 6 Age regression of pyrotechnic control cable current attenuation at 10 MHz frequency.

intersection of the 3-sigma prediction limit and ageout alert limit, but documentation is available to show that a wide safety margin exists. The present data therefore, is not considered to be indicative of a potential life-limiting problem.

Summary and Conclusions

The present evidence offers very high confidence that the Minuteman Stage IIIa will meet its 3-yr storage requirement easily without maintenance. There is considerable margin for aging, and in all but two cases, it does not appear likely that this margin will be dissipated within the 10-year design objective. In the two cases in which this statement cannot be made categorically, further operating margins are evident upon closer examination.

Accuracy of Orbit Determination from Ionospherically Corrupted Tracking Data

P. NORRIS*
European Space Research Organization, Toulouse, France

Nomenclature

De	= ionospheric maximum electron density, el/m^3
f_m, f_R, f_{RR}	= radio frequency of the interferometer, range, and range-rate signals, respectively, Hz
He	= height at which De occurs, km
L	= logarithm to the base ten of De
l, m	= interferometer direction cosines
$\Delta l, \Delta m$	= ionospheric effects on l and m
RG	= geocentric radius of the ground station, km
ρ	= range of the satellite relative to the ground station, km
$\Delta\rho, \Delta\dot{\rho}$	= ionospheric effects on range and range rate, respectively, m, m/s
$\theta, \dot{\theta}$	= elevation angle of the satellite from the ground station, and its rate of change, rad, rad/sec

I. Introduction

TRACKING data at frequencies in the region of 150 MHz (vhf) are commonly used for tracking satellites. These data are significantly affected by passage through the ionosphere. Predicting the accuracy with which the satellite orbit can be determined using the vhf data has been a problem in the past because of the lack of an ionospheric model whose statistical behavior can be introduced into the usual orbit determination accuracy software. Previous studies have: a) assumed a constant large error,[1] b) treated worst-case situations only,[2] or c) assumed a percentage error on the ionospheric effect.[3]

This study introduces a procedure whereby the ionosphere is modeled by a single parameter whose statistical distribution is approximately normal. This parameter is then included in the solution vector along with the satellite position and velocity (state vector). Unlike methods a), b), or c) this procedure

Received April 15, 1974; revision received July 15, 1974.
Index categories: Spacecraft Tracking; Spacecraft Navigation, Guidance, and Flight-Path Control Systems.

* Mission Analyst, METEOSAT Program Office.

establishes whether the ionospheric errors can be removed from the tracking data, and, if so, what the effect on orbit determination accuracy is.

The procedure is demonstrated by application to Goddard Range and Range-Rate (GRARR) data for two phases of a synchronous satellite mission: the transfer orbit phase (TO) and the synchronous orbit phase (SO). A third example is also shown using interferometer data for the TO case.

II. GRARR Error Model[4]

As their name implies, GRARR data consist of nearly simultaneous measurements of the range and range rate of a satellite with respect to a ground station. They are available at two different frequencies: S-band (~2 GHz) and vhf. S-band GRARR data are relatively unaffected by the ionosphere, and so are not considered here. The information in the GRARR data is assumed to be corrupted by a bias (15 m 1σ uncertainty for range, 0.1 m/sec for range rate), a timing error (0.003 sec), geodetic errors (15 m in each coordinate), ionospheric errors (Section IV), a range-rate drift (10^{-4} m/sec^2) and noise (10 m, 0.1 m/sec in low orbit, 0.2 m/sec in high orbit). This model is based on experimental work by several investigators.[5-7]

III. Interferometer Error Model[8]

The interferometer data are assumed similar to those obtained from the NASA "Minitrack" or CNES Diane network. A station in these networks consists of two antenna pairs, aligned north-south and east-west, which receive signals from a vhf beacon on a satellite. The antenna pairs produce phase difference measurements which can be conveniently visualized as giving two direction cosines of the satellite relative to the station.[13]

These direction cosines are assumed to be corrupted by timing, geodetic and ionospheric errors as for GRARR, and by baseline azimuth and elevation errors (1σ uncertainty = 50 μrad each), a baseline scale error (5.10^{-5}), a frequency error (150 Hz) and noise (10^{-4}). The model is based on experimental work at the NASA Goddard Space Flight Center.[9,10] Note that the degradation of the noise value, as satellite to ground range increases, is ignored. Also, the use of the antenna sidelobes for data reception (a possible operational mode with Diane) is excluded.

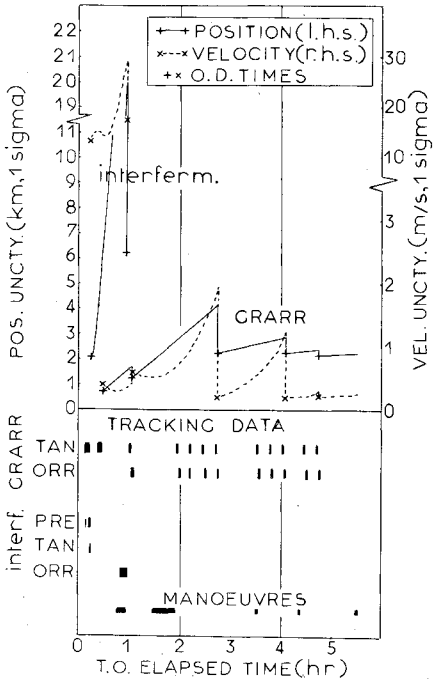

Fig. 1 Total position and velocity uncertainty in the transfer orbit cases.

IV. Ionosphere Model

For a satellite above the ionosphere, and elevation angles greater than 5°, the ionospheric effect on range can be expressed (to better than 1 m accuracy at very-high frequencies), using Willman's ionospheric model, as [11,12]

$$\Delta\rho = \frac{-5.4.10^4 De(He-50)}{f_R^2\left\{1-\left(\frac{RG\cos\theta}{RG+50}\right)^2\right\}^{1/2}} \tag{1}$$

The range-rate effect is given by[12]

$$\Delta\dot{\rho} = \frac{\Delta\rho RG\dot{\theta}\sin\theta\cos\theta {f_R}^2}{(RG\sin^2\theta+100){f_{RR}}^2} \tag{2}$$

The direction cosine effect is derived from formulas of Bean and Thayer,[13] again using Willman's electron density vs height profile,

$$\Delta l = \frac{-166.10^3 Del(He-50)(RG\sin\theta+\rho)}{RG\rho {f_m}^2\sin^2\theta} \tag{3}$$

$$\Delta m = m\Delta l/l$$

Since De can vary by more than an order of magnitude in either direction, its logarithm L is used in the error model equations instead. The a priori uncertainty assigned to L is 0.5. This implies that there is about a 5% chance of De differing from its expected value by more than an order of magnitude—in general agreement with observed conditions.[12]

The characterization of the ionosphere by a single parameter has been shown to be reasonable for periods of the order of 20 min.[11,14] In this study, a separate L parameter is introduced for each separate orbit determination in the TO cases (max time span = 50 min) with the same parameter being used for all stations. In the SO cases, a separate L parameter is introduced for each one hour of data, and for each station, and adjacent parameters are assumed to have a priori correlation of 0.83.[3]

Several techniques are available for removing the ionospheric effects from vhf tracking data (e.g.: multiple frequencies, range vs range-rate comparison, Faraday rotation[15]). When such techniques are used, the uncertainty in L becomes much smaller (perhaps even zero), although the data noise may be increased.

V. VHF-GRARR Transfer Orbit Case

The case in question corresponds to the proposed flight plan for the METEOSAT mission, in which a Thor-Delta 2914 launch vehicle from Cape Kennedy places the spacecraft in a transfer orbit whose characteristics are as shown in Table 1. Several attitude maneuvers are performed prior to the first apogee. Orbit determination (OD) information is required prior to each maneuver, and is in turn corrupted by the maneuver.

It is assumed that a sequential processing technique[16] is used. Tracking data are obtained from stations in Madagascar (TAN) and Australia (ORR) (coordinates in Table 2) for $2\frac{1}{2}$ min/station/

Table 1 Transfer orbit characteristics

Apogee radius	42353 km
Perigee radius	6563 km (altitude = 185 km = 100 nm)
Inclination	28.78°
Argument of perigee	180°
Longitude of first equator crossing	−6.5°
Period	634.45 min

Table 2 Station coordinates

	TAN	ORR	PRE	NEU
Geocentric radius, km	6377	6372	6374	6366
Geocentric latitude, deg	−19.0	−35.6	−25.6	49.8
East longitude, deg	47.3	148.95	28.4	5.1

Table 3 Ionospheric parameter recoverability

	GRARR					Interferometer	
OD no.	1	2	3	4	5	1	2
Postfit uncertainty on $L(1\sigma)$	0.002	0.12	0.03	0.11	0.09	0.2	0.1

15-min period,† provided the elevation angle is greater than 15°. One measurement (range plus range rate) is simulated every 15 sec.

Data for OD is taken up to ~20 min prior to each maneuver. After the maneuver, the covariance matrix produced by the previous OD has its velocity components "corrupted," and this matrix is then used as the a priori matrix for the next OD. Five ODs are thus needed to cover the transfer orbit.

The time history of total position and velocity determination accuracy (1σ) is in Fig. 1. The tracking periods and times of maneuvers are also shown. After completion of each OD, the covariance matrix is propagated forward until the time of the next OD. It is clear that very small quantities of data give tolerable accuracy. The first OD contains just 40 data points from TAN and gives total position accuracy of ~1 km. The uncertainty in satellite position based on the launcher dispersions (i.e., assuming no tracking data are available) is ~30 km after 1 hr.

The error model parameters are not so easily determined. Range bias, range-rate bias, range-rate drift, and geodetic errors are not recovered to any significant extent. So, the effect of those errors on the OD results is a function of their a priori uncertainty values.

Timing biases and ionospheric parameters are recovered, however. The timing bias uncertainty is reduced to about 0.01 msec after the first OD. A separate L parameter is introduced for each OD. The 1σ value after each OD is shown in Table 3. The ionospheric effects are clearly separable from orbital perturbations at the start of the TO, but are less so at the end.

VI. Interferometer Transfer Orbit Case

Interferometer data are assumed to be provided by three tracking stations: TAN, ORR,‡ and PRE (South Africa; see Table 2). The Table 1 orbit is again used. The interferometer has a fan-shaped beam which restricts visibility of a satellite to periods when it is less than five sky-angle degrees off the east-west or north-south axes of the ground station. This reduces the interferometer tracking coverage in the TO to the first hour of the orbit. The five OD's of the range/range-rate case are thus reduced to two.

Figure 1 shows the results; note the change of scale for the velocity results. The early tracking data from TAN and PRE are processed in 1 OD run. This produces satellite position uncertainty (1σ) of about 2 km, but velocity uncertainty of about 13 m/sec. This latter result causes a rapid degradation in the position accuracy, so that by the time the next set of data is taken at ORR, the position uncertainty is about 30 km. The inclusion of the ORR data reduces this to less than 7 km and gives velocity uncertainty of 18 m/sec, but unfortunately this information is coincident with an attitude maneuver (see Fig. 1) and so is of little practical use. The ionospheric parameters are partially recovered in these OD runs (see Table 3), but other measurement error model parameter uncertainties retain their a priori values.

VII. VHF-GRARR Synchronous Orbit Case

The synchronous orbit case assumes a circular, near-equatorial geosynchronous orbit with the satellite centred at 0° longitude. VHF-GRARR data are assumed to be taken at a rate of 1 point/min from each of two stations (TAN and NEU, Belgium, see Table 2) for three hours. Preliminary studies had shown that nonzero inclination, eccentricity, and longitude§ values give better accuracy, so the orbit used is essentially a worst-case situation.

Table 4 VHF-GRARR synchronous orbit results

			Resulting uncertainty (1σ)			
Run	Range-rate accuracy (m/sec, 1σ)	Uncertainty in s/c spin	Longitude (m)	Total position (m)	Total velocity (cm/sec)	L
1	0.2	Yes	108	207	0.81	0.02
2	0.2	No	44	176	0.60	0.01
3	10	Yes	5000	5100	9.68	0.4

Results of three runs of interest are shown in Table 4. Run 1 corresponds to the error model described in Sec. II. Run 2 differs only in assuming that range-rate errors due to satellite rotation uncertainty are zero: accuracy is improved by about 15% compared to Run 1. Run 3 assumes that range-rate data are grossly inaccurate: position and velocity determination accuracies are considerably worse than for Run 1. This is caused by the inability of the tracking data to separate the ionospheric parameter errors from the orbital errors—especially longitude and rate of change of latitude. Range-rate data from a geostationary satellite are unaffected by the ionosphere [in Eq. (2) $\dot{\theta} = 0$] so, when present, these data permit the separation of ionospheric errors from orbital errors. This is shown in the right-hand column of Table 4 where the a posteriori uncertainty in the L parameter is shown (a priori value was 0.5 for all runs). Previous studies[3,17] on this topic concluded that range-rate data are not nearly as useful as range data for determining a geostationary orbit. This conclusion was caused either by assuming that ionospheric errors were not present in the tracking data, or by overly simplified modeling of those errors.

References

[1] Walter, H. G., "Accuracy Estimation for Spacecraft Position and Velocity," SR-16, May 1971, ESRO, Darmstadt, Germany.

[2] Anderson, R. E., "Final Report on Phases 1 and 2 VHF Ranging and Position Fixing Experiment Using ATS Satellites," S-71-1109, STAR N72-16510, May 1971, General Electric Company, Schenectady, N.Y.

[3] Conrad, D. A., "Error Analysis of Navigation Satellite System," *Automatic Control in Space 3*, IFAC, Paris, France, 1970, pp. 779–796.

[4] Norris, P., "Error Model for VHF Goddard Range and Range Rate Data," EWP-804, Feb. 1974, ESRO, Noordwijk, Holland.

[5] Berbert, J. H., Maresca, P., Norris, P., and Reich, R., "Intercomparison of Collocated Laser Optical and GRARR Radio Ranging System Tracks on Geos-A," X514-67-447, STAR N67-39092, Sept. 1967, NASA.

[6] Gross, J. E., "Preprocessing Electronic Satellite Observation," CR-1183, STAR N69-11740, Nov. 1968, NASA.

[7] Marini, J. W. and Murray, C. W., Jr., "Effect of Satellite Spin on Explorer 33 and 35 Doppler Tracking Data," X551-69-52, STAR N69-20896, Feb. 1969, NASA.

[8] Norris, P., "Coed—A Computer Program for Analysis of Orbit Determination Accuracy using Simulated Tracking Data," EWP-805, March 1974, ESRO, Noordwijk, Holland.

[9] Rosenbaum, B., "Analysis of Minitrack Residuals," TM X-65650, STAR N71-32406, Dec. 1970, NASA.

[10] Brown, D. C., "Metric Analysis of Minitrack Optical and Interferometer Data," CR-122396, STAR N72-24867, June 1971, NASA.

[11] Brown, D. C., "Advanced Techniques for the Reduction of Geodetic SECOR Observation," Final Rept., Contract DA-44-009-AMC937(X), STAR N67-15035, July 1966, DBA, Inc, Eau Gallie, Fla.

[12] Berbert, J. H. and Parker, H. C., "Geos Satellite Tracking

† This restriction is caused by the inability of the satellite to receive telecommands while tracking is in progress.

‡ The satellite range when in view of ORR is 14,000 km. This is at the outer limit of minitrack capability, so this data pass is of doubtful reliability.

§ Actually, longitude = 20°E is the worst case for the chosen ground station configuration.

Corrections for Refraction in the Ionosphere," X514-70-467, STAR N72-18852, Dec. 1970, NASA.

[13] Schmid, P. E., "NASA Minitrack Interferometer Refraction Correction," TN D-5966, STAR N71-18565, March 1971, NASA.

[14] Mallinckrodt, J., Parker, H. C., and Berbert, J. H., "Refraction Studies Using the WICE Data," *Proceedings of the Geos-2 Program Review Meeting*, Vol. 2, Nov. 1970, TM X-67272, STAR N71-31847, NASA.

[15] Norris, P., "VHF Satellite Tracking Data Errors—Considerations for ESRO Projects," ESTEC Memo NOG/2092/N/11/mc, Aug. 1973, ESRO, Noordwijk, Holland.

[16] Rourke, K. H. and Jordan, J. F., "Application of Sequential Filtering to Estimation of the Interplanetary Orbit of Mariner 9," *Journal of Spacecraft and Rockets*, Vol. 10, No. 12, Dec. 1973, pp. 773–778.

[17] Norris, P., "Surveillance Accuracy in the Aerosat System," TN-87, STAR N74-16368, June 1973, ESRO, Noordwijk, Holland.

Slot Heating Associated with Roll Control Fins

T. Taz Bramlette*
Sandia Laboratories, Livermore, Calif.

Nomenclature

b = skin thickness
c = heat capacity
d = slot depth
L = model length
M = Mach number
$\dot{q}$ = heat-transfer rate
$Re_{\infty,L}$ = freestream Reynolds number based on model length
Re_τ = friction Reynolds number, $(\tau_w/\rho_e)^{1/2}(\rho_e w/\mu_e)$
T = temperature
t = time
w = slot width
y = slot depth coordinate
μ = viscosity
ξ = angular coordinate
ρ = density

Subscripts
o = stagnation
w = wall
∞ = freestream

Introduction

ONE means of controlling the roll rate of small re-entry vehicles consists of fins located near the base of the vehicle. Installation of these fins, however, results in a circular slot of varying depth in the heat shield, which presents a potential aerothermal design problem. The desirability of a wide slot to minimize the probability of binding conflicts with the need for a narrow, deep slot to minimize the heat input to the fin actuation mechanism. Moreover, the effect of the complex flowfield that exists in the region near the fin on slot heating is not known. The present results were obtained as part of an experimental study of the aerothermodynamics associated with small fins in laminar, hypersonic flow.[1]

Facility, Model, and Experimental Technique

The tests were conducted in the Air Force Flight Dynamics Lab. (AFFDL) High Temperature Facility,[2,3] which is a hypersonic blowdown wind tunnel. Nominal test conditions were $M_\infty = 10$, $Re_{\infty,L} = 1 \times 10^6$ ($Re_\tau \approx 90$), and $T_w/T_o = 0.27$. The model was a 7° half-angle sharp cone which had small fins mounted near its base. For the slot heating tests the fin was swept 60° from the normal, had a cylindrical leading edge, and a length, height and width of 1.83, 0.5, and 0.3 in., respectively. The fin was surrounded by a circular slot which had a width of 0.05 in. and a depth which varied from 0.51 in. to 0.75 in. The walls of the slot were constructed of stainless steel ($b = 0.030$ in.) and instrumented with Chromel-Alumel thermocouples. A sketch of the model and the thermocouple locations are presented in Fig. 1.

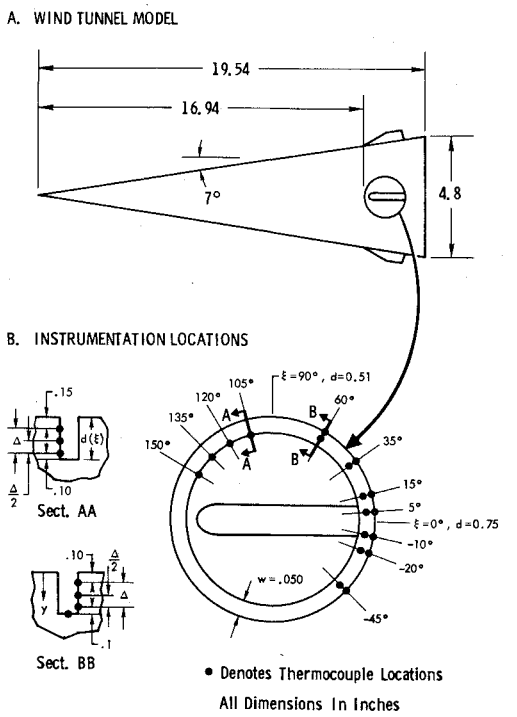

Fig. 1 Sketch of wind-tunnel model.

Thermocouple data were taken at a sampling rate of 57 times/sec when the model reached the flowfield core. The heat transfer rate was obtained from the relation

$$\dot{q} = \rho c b (dT/dt)$$

In general, the temperature rise was less than 40°R. Consequently, no correction for surface conduction or radiation was made.

Results

Figure 2 presents results which are influenced by the flowfield in the fin/cone corner region. The heat transfer rate has been

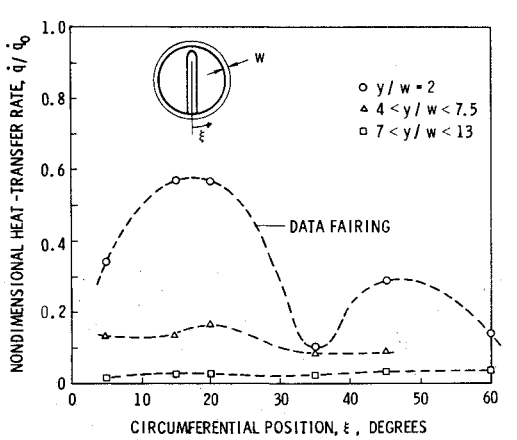

Fig. 2 Slot heating for different circumferential positions.

Received May 9, 1974; revision received July 12, 1974. This work was supported by the U.S. Air Force and the U.S. Atomic Energy Commission.

Index categories: Supersonic and Hypersonic Flow; Viscous Nonboundary-Layer Flows.

* Member of Technical Staff, Systems Development Division. Member AIAA.